Axiotaxy and epitaxial textures in C54-$TiSi_2$ films on Si(001) and Si(111) substrates

F.A. Geenen[a], J. Jordan-Sweet[b], C. Lavoie[b], C. Detavernier[a]

[a]*Department of Solid-State Sciences, Ghent University, 9000 Gent, Belgium*
[b]*IBM T.J. Watson Research Center, Yorktown Heights, NY, USA*

Abstract

Titanium silicide can be used in micro-electronic applications to reduce the contact resistance for Silicon-based transistors. This paper gives an overview of the preferred orientation between the Ti-silicide films and Si(001) and Si(111)-oriented substrates. We report on several axiotaxial alignments, which are observed in addition to the previously known epitaxial alignments. The axiotaxial textures can be related to the epitaxial one and its stability is interpreted through plane-to-plane alignment across the interface. Reducing the Ti film thickness from 30 to 8 nm favours the epitaxial alignment instead of the axiotaxial alignments.

Keywords: titanium silicide, epitaxy, axiotaxy, texture, C54-$TiSi_2$

1. Introduction

Metal silicides are extensively used in micro-electronics for contacting the source and drain regions of Si-based transistors [1]. C54-$TiSi_2$ was introduced in Complementary Metal Oxide Semiconductor (CMOS) devices for ultra-large scale integration during the early 90's and has subsequently been replaced by sequentially $CoSi_2$ and NiSi for high-performance applications [2]. C54-$TiSi_2$ is still being used in traditional planar CMOS technology for applications with high reliability demands, e.g. the automotive industry or high temperature

Email address: filip.geenen@ugent.be (F.A. Geenen)

Table 1: Overview of epitaxial orientations reported in the literature for orthorhombic C54-$TiSi_2$ films on Si(001) and Si(111) substrates.

Substrate	**1st alignm.**	**2nd alignm.**	**Ref.**
Si(111)	$(100)//(111)$	$[004]//[02\bar{2}]$	[14][15][16]
	$(001)//(111)$	$[400]//[0\bar{2}2]$	[14][15][16]
	$(101)//(111)$	$[31\bar{3}]//[2\bar{2}0]$	[15][16]
	$(010)//(111)$	$[001]//[1\bar{1}0]$	[15]
	$(\bar{2}\bar{1}1)//(111)$	$[1\bar{1}1]//[1\bar{1}0]$	[15]
Si(100)	$(10\bar{1})//(\bar{1}11)$	$(\bar{3}\bar{1}\bar{3})//(01\bar{1})$	[17]
	$(\bar{1}\bar{3}0)//(\bar{1}\bar{1}1)$	$(004)//(1\bar{1}0)$	[17, 18]
	$(10\bar{1})//(\bar{1}11)$	$(121)//(110)$	[17]

applications. In recent years, Ti-based contacts have regained considerable at-
10 tention for implementation in FinFET-technology through the formation of a thin Ti-Si compound, where Ti-based contacts offer a significant advantage over Ni because of the lower mobility of Ti in Si [3, 4, 5, 6, 7, 8].

Silicide films for CMOS applications are usually formed through a solid-state reaction, where a thin metallic film is deposited on a Si substrate and
15 subsequently heated to form a silicide compound [2]. The solid-phase reaction often induces a preferential crystallographic orientation between the formed silicide film and the single-crystal Si substrate. Crystalline texture is known to affect functional properties such as the morphological stability [9, 10, 5, 6, 11] and interface contact resistance [12] of the silicide film. The texture of several
20 metal silicides has therefore been studied in detail over the past decades [13].

Most texture studies on titanium silicides were performed during the 90's and focused on the epitaxial orientation of the $TiSi_2$ film with the substrate [14, 15, 16, 19, 17, 20]. Several epitaxial orientations were reported (Table 1) and their origin was discussed within the frameworks of geometric-based
25 models such as the 0-lattice [15] and edge-to-edge matching models [21] or by simply overlaying the atomic structure of both film and substrate [17]. However,

the transformation of C54-$TiSi_2$ from a C49-$TiSi_2$ phase is nucleation-driven and as a result the C54-nucleated film often heavily granulated. More recent research on C54-$TiSi_2$ focuses on the epitaxial alignment between the nucleated alignment of the C54-nucleated film and the underlying Si substrate in order to improve the morphology of such C54 films [6, 7, 8, 18]. Since then the improvement of the used experimental techniques have led to the discovery of other types of texture, such as axiotaxy [22] and also a particular plane rotation across crystalline grains of Ni-Si compounds termed trans-rotational domains [23], rendering novel insights on how the texture of the silicide film affects its stability. A recent review by Deschutter *et al.* [13] provides an overview on the complex textures possible in such thin-film systems. Currently, no publications are available that investigates these novel texture-types for $TiSi_2$-thin films in great detail, since the texture of $TiSi_2$ was mostly researched prior to their discovery.

This paper reports on the axiotaxial nature of C54-$TiSi_2$ films on both Si(001) and Si(111) substrates. Synchrotron X-Ray-Diffraction (XRD) pole-figure measurements reveal the presence of multiple axiotaxial features and their importance in interpreting the different previously-reported epitaxial orientations.

2. Experimental methods

Ti films with a thickness of 8 and 30 nm were deposited using Physical Vapor Deposition (PVD) on commercially-available Si substrates. Two orientations of Si substrate were used: Si(001) and Si(111) (the latter substrate had an intentional miscut of 0.3°, as observed through the offset between the sample optical reflection normal and the crystalline diffraction normal). Both substrates received a short HF dip prior to loading in the deposition chamber. Ti was sputtered in an Ar atmosphere with a pressure of 1.33×10^{-3}Torr, after a base pressure of 1×10^{-7}Torr had been reached in a Materials Research Corporation PVD system. A 8 nm TiN capping layer was subsequently deposited on the Ti

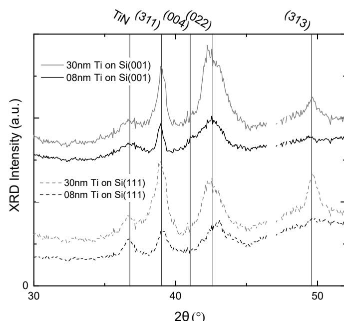

Figure 1: The total diffraction intensities as a function of diffraction angle 2θ. Data was extracted from pole-figure XRD measurements at the X20A beamline of the NSLS synchrotron with an x-ray energy of 8.0 keV. The intensity of the Si substrate (220) diffraction near 47° was masked due to a to high intensity for the detector.

film without breaking the vacuum in order to protect the film from oxidation after the deposition process.

Samples of at least $1\,\mathrm{cm}^2$ were subsequently heated in a purified He atmosphere at a constant rate of $3\,°\mathrm{C\,s}^{-1}$ at the *in situ* heating set-up of the X20C beamline at the National Synchrotron Light Source (NSLS, Brookhaven National Laboratory). Atomic Force Microscope images of the surface of these samples taken with a Brucker Edge system (i.e. the TiN capping layer) show a rough surface, with an $\mathrm{R}_a \approx 3.5\,\mathrm{nm}$, independent of the substrate or film thickness. Grazing incidence rocking curve measurements were obtained with a Brucker D8 X-Ray Diffraction (XRD) with an 2θ angle of 0.3° with a stepsize of 2 arcsec. The bare substrates had a full-width-half-maximum (FWHM) value of 68 and 70 arcsec for respectively the Si(100) and Si(111) substrates, whereas FWHM value of 80 and 84 arcsec were obtained for annealed 8 and 30 nm Ti films on both substrates.

X-Ray Diffraction (XRD) pole-figure measurements were performed to determine the silicide's texture. The C54 crystalline structure (JCPDS No. 00-035-0785)was confirmed through these measurements (Fig. 1). Pole figures are obtained by measuring the diffraction intensity from a set of crystallographic

(a) Si(001)

(b) Si(111)

Figure 2: Orientation of the pole-figure maps are fixed with respect to the substrate orientation, as shown in this figure.

planes at a fixed diffraction angle 2θ, while tilting and rotating the sample both in-plane and out-of plane, respectively parametrised by the angles ϕ for the azimuth and χ for the elevation angle [24]. The diffraction angle 2θ is related to a specific $\{hkl\}$ lattice plane of a certain crystalline phase through Bragg's law of diffraction. The measured diffraction intensity I for a specific $\{hkl\}$ plane is dependent on the angles ϕ and χ, as I scales with the crystalline volume for which the $\{hkl\}$ plane is oriented along those angles ϕ and χ. Thus a polar plot of $I(\phi,\, \chi)$ correlates with a statistical distribution of the preferred orientation of the corresponding $\{hkl\}$ plane, covering all grains illuminated by the incident X-rays (which had an area of ca. $1.5\,\mathrm{mm}^2$). Pole figures therefore offer a significant statistical advantage in comparison with TEM-based texture research, where the number of grains measured and investigated are significantly limited.

In this work, pole figures were measured at the X20A synchrotron beamline of the NSLS, using an x-ray wavelength of $\lambda = 0.154$ nm, as selected using a Ge(111) monochromator. The diffracted x-rays were detected using a custom linear detector (8 cm Si strip detector, 640 pixels) which allows the simultaneous acquisition of pole figures covering 20 to 60° in 2θ, which includes diffraction of the (311), (313), (202), (004) and (022) planes of orthorhombic C54-$TiSi_2$

(JCPDS No. 00-035-0785). The pole figures were acquired in steps of 1.0° in ϕ and χ ($0 \leq \chi \leq 85°$ and $-10 \leq \phi \leq 100°$ for Si(100) or $-10 \leq \phi \leq 130°$ for Si(111)). Complete pole figures were obtained by extending the measured
95 data to the full range $0 \leq \phi \leq 360°$, taking into account the symmetry of the substrate. The samples were oriented so that the Si poles are located at the ϕ and χ coordinates as displayed in Fig.2. The diffracted intensity is represented by a stereographical projection for χ and ϕ, and by using a logarithmic gray-scale map, where white and black represent respectively a low or high intensity. A
100 more detailed description of pole-figure measurements and their analysis can be found in earlier works describing the formation and texture of NiSi [22, 24, 25]. The pole figures were analysed using the GUSTAV [26] software package.

3. Results and discussion

In the following paragraphs we categorise the observed features on the mea-
105 sured pole figures into texture components. The observed features are discussed for the (311) and (313) planes of the orthorhombic C54-phase (a=8.26 Å, b=4.79 Å and c=8.55 Å). These two planes allows a clear interpretation because there is no diffraction from other planes having a similar inter-planar distance. Texture components are proposed which explain the observed features and the
110 analysis was corroborated by pole figures for the C54-$TiSi_2$ (202), (004) and (022) planes (not shown here).

3.1. Texture on Si(001)

The recorded pole figures for C54-$TiSi_2$ films on Si(001) clearly contain several non-random patterns (Fig. 3), indicating preferential alignment with the
115 substrate. Circular features can be associated with *axiotaxy* and dotted features with *epitaxy*. The fact that these epitaxial features are overlapping with some of the axiotaxial circles suggests that the two types of texture components are inter-related and will be discussed further. Figure 4 shows the diffraction intensities for regions in ϕ and χ, selected specifically to represent the different

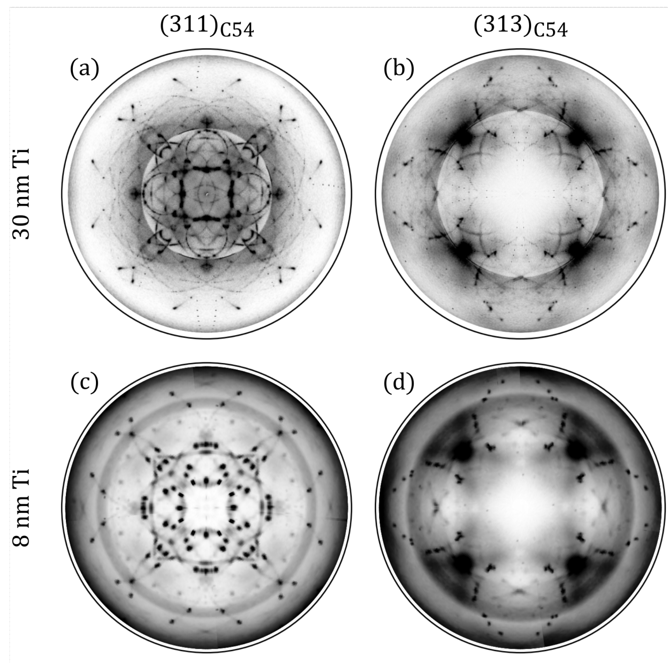

Figure 3: Pole-figure data for C54-$TiSi_2$ (311) and (313) diffraction planes for samples with an as-deposited Ti thickness of 30 nm (**a, b**) and 8 nm (**c, d**) on Si(100).

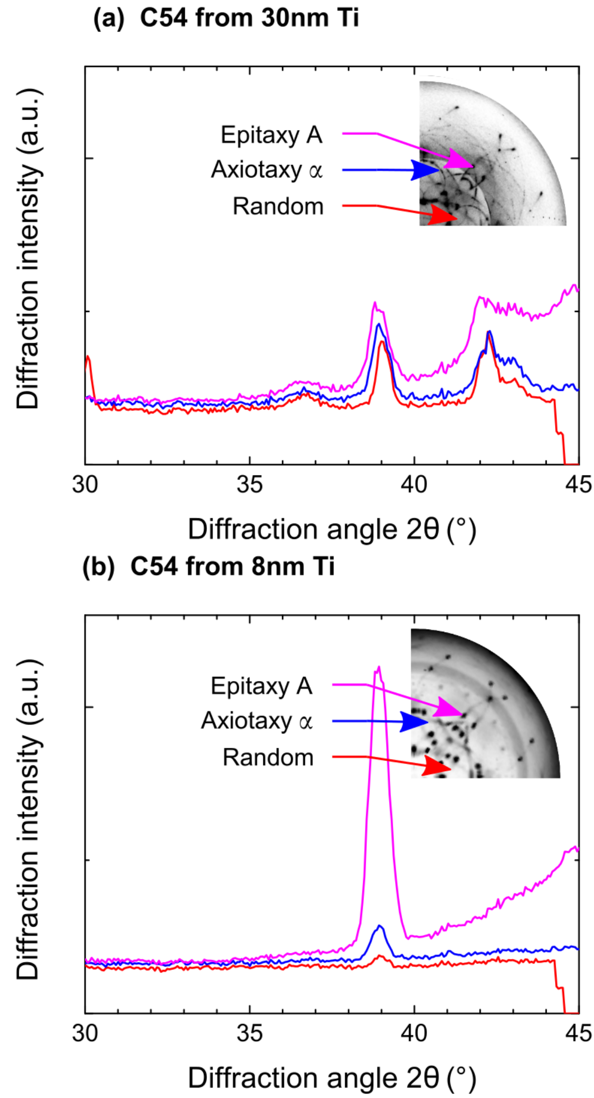

Figure 4: The diffraction intensity plotted for selecting specific regions in both ϕ and χ, associated with axiotaxy, epitaxy and random distribution of the grains' orientations. The regions in ϕ and χ are selected for the diffraction at $2\theta = 39.1°$ (i.e. C54-$TiSi_2$ 311).

120 textures as oriented for the C54-$TiSi_2$ 311) plane. It is clear that the randomly-oriented grains represent a lower fraction of the film when going from 30 to 8 nm as-deposited Ti thickness, and that a relatively larger fraction of the C54-film is oriented along the epitaxial texture. .

Axiotaxial alignment

125 In general, circular patterns on a pole figure are generated by either an axiotaxial or a fiber alignment between the film and the substrate. Both textures require one of the film's planes to have a fixed orientation with respect to the substrate. The direction perpendicular to these planes then acts as an axis of rotation, and every individual grain is oriented as a random rotation around 130 this axis of symmetry. By consequence, diffracting planes which are inclined to this axis of rotation will result in circular features on the associated pole figure.

Two different kinds of circular texture features are reported in literature: *fiber* and *axiotaxial*. The axis of rotation for a fiber alignment is always perpendicular to the substrate surface, and by consequence the diffraction rings 135 are always concentric on the pole figures. An axiotaxial alignment does not have this restriction, and by consequence the non-concentric circular features in figure 3 indicate axiotaxial texture. The pole-figure measurement was paused for some time in order to increase the synchrotron X-rays intensity, resulting in a discontinuity in diffraction background, with a lower (whiter) background 140 around the center of the pole figure and a higher (darker) background at the edge of the pole figure.

The axiotaxial texture can occur when planes from the film and the substrate have a similar inter-planar distance and orientation. This allows a plane-to-plane match across the interface, and the axiotaxial features are uniquely defined by 145 identifying these matching planes. A total of four different axiotaxial relationships allow us to reconstruct the complex pattern of observed circular features in figure 3: $(404)_{C54} \sim//(222)_{Si}$ (Fig. 5a, b), $(404)_{C54} \sim//(113)_{Si}$ (Fig. 5c,d), $(511)_{C54} \sim//(113)_{Si}$(Fig. 5e,f) and $(115)_{C54} \sim//(113)_{Si}$ (Fig. 5g,h) .

Axiotaxy originates from a plane-to-plane match across the interface between

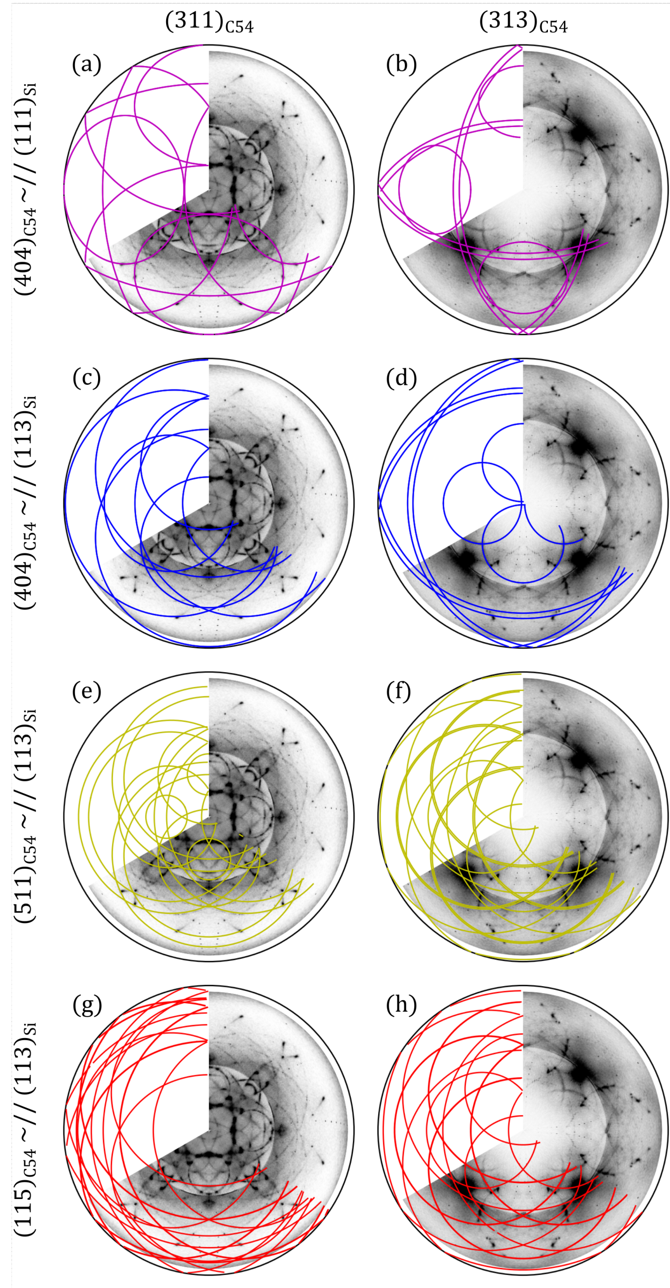

Figure 5: $(311)_{C54}$ and $(313)_{C54}$ pole figures of a C54 $TiSi_2$ layer with an as-deposited Ti thickness of 30 nm, overlayed with axiotaxial features related to matching of specific $TiSi_2$ planes with the (111) (**a**, **b**) and (113) (**c,d,e,f,g,h**) planes of Si across the interface.

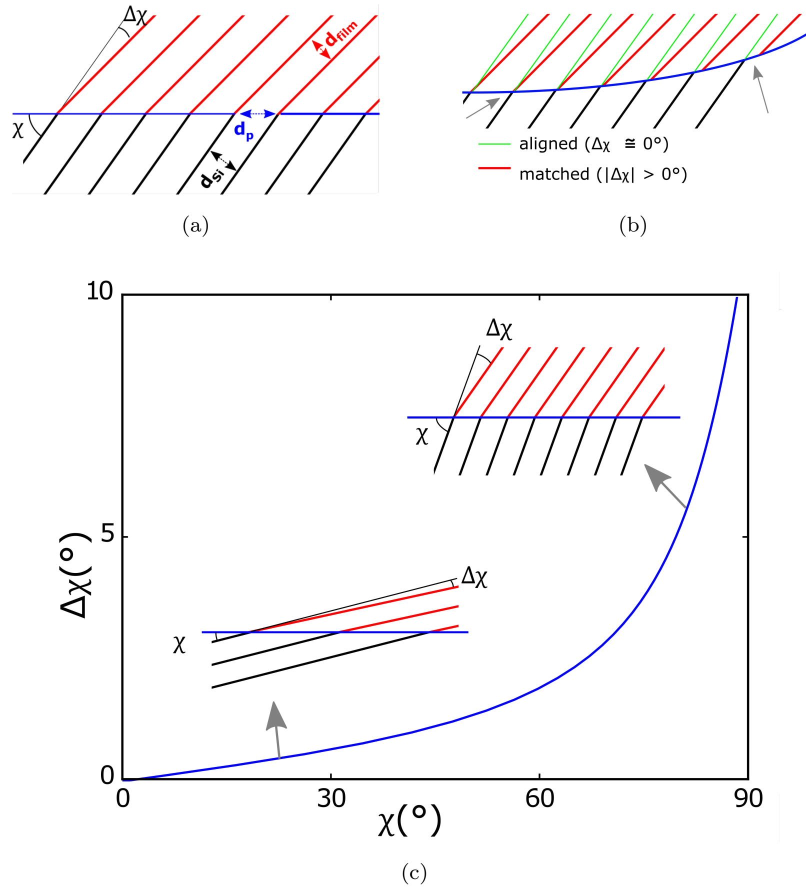

Figure 6: To achieve axiotaxial match between at a flat interface (**a**), the difference in planar distance between d_{Si} and d_{film} can be compensated by a slight tilt $\Delta(\chi)$, resulting in an identical projected spacing d_p at the interface to achieve plane-to-plane match. At a rougher interface (**b**), small values of $\Delta(\chi)$ are more stable to roughening of the interface [22]. In addition, the angle required to compensate a given difference in d-spacing (e.g. $d_{Si} = 1.02 \cdot d_{film}$) is also dependant on the inclination angle χ of the substrate plane with the interface, (**c**).

Table 2: Fitted axiotaxial texture components between C54-$TiSi_2$ and Si(001) substrate. A difference in d-spacing between the film and substrate planes will result in a mismatch at the interface. The small difference in d-spacing (D) between the axiotaxial component and the substrate can be compensated at the interface through a small tilt in χ.

	Matching planes	χ_{exp} (°)	$\Delta(\chi)_{exp}$ (°)	**d** (Å)	Δ d (%)	χ_{th} (°)	$\Delta(\chi)_{th}$ (°)
	Si(222)	-	54.7	1.57	-	54.7	-
$\alpha_{Si(100)}$	C54(404)	51.5	3.2	1.51	4.2	51.5	3.2
	Si(113)	25.2	-	1.64	-	25.2	-
$\alpha'_{Si(100)}$	C54(404)	23.4	1.8	1.51	8.2	23.0	2.2
$\beta_{Si(100)}$	C54(511)	24.0	1.2	1.56	5.2	23.8	1.4
$\gamma_{Si(100)}$	C54(115)	24.5	0.7	1.60	2.5	24.6	0.6

film and substrate. The quality of this match is often discussed in the literature with respect to the small difference in the planar distance between these to two matching planes, typically less than 5 %[22, 10, 27, 13]. It is then remarkable that the (404) plane of $TiSi_2$ would not only match with $(222)_{Si}$ ($\Delta d = 4.2\,\%$) but also with $(113)_{Si}$ ($\Delta d = 8.2\,\%$). Nevertheless, Detavernier *et al.* [22] argue that a mismatch in d-spacing can be compensated by a small tilt in χ of the orientation of the film's axis of rotation, resulting in a matching *projected* planar distance d_p on the interface (Fig. 6a). We in fact observe that all axiotaxial features are slightly tilted around the Si(222) and Si(113) poles ($\Delta(\chi)_{exp}$ in Tab. 2). However, Detavernier *et al.* also point out that a high tilt $\Delta\chi$ can in principle always force plane-to-plane matching across a perfectly planar interface, this match quickly vanishes along a realistic interface which includes non-planarity and interfacial roughness (Fig. 6b). This can be expected to be particularly important during the nucleation of a new phase during a solid-state reaction, which is exactly when the grain orientation will be selected. We here add to this discussion that $\Delta\chi$ not only is dependant on the difference Δd, but is also dependant on the inclination angle χ of the rotation axis with respect to the

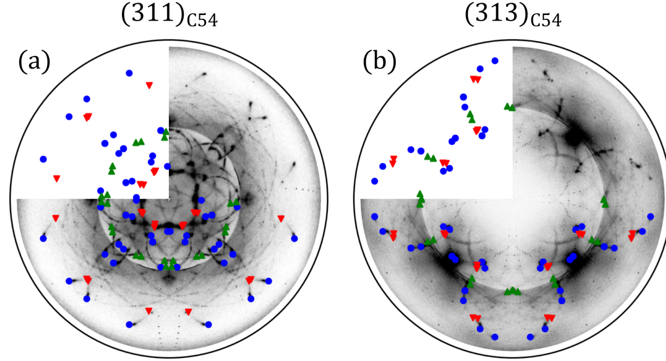

Figure 7: Pole figures overlayed with identified epitaxial features for data from a C54-$TiSi_2$ sample with an as-deposited Ti thickness of 30 nm.

Table 3: Overview of observed epitaxial components of C54-$TiSi_2$/Si(001).

Epitaxy (Symb.)	1st alignm.	2nd alignm.
$A_{Si(001)}$ (●)	$(101)_{C54} \sim//(111)_{Si}$	$(\bar{3}\bar{1}3)_{C54} \sim//(\bar{1}01)_{Si}$
$B_{Si(001)}$ (▼)	$(101)_{C54} \sim//(111)_{Si}$	$(1\bar{1}\bar{1})_{C54} \sim//(\bar{1}10)_{Si}$
$C_{Si(001)}$ (▲)	$(5\bar{1}1)_{C54} \sim//(11\bar{3})_{Si}$	$(400)_{C54} \sim//(001)_{Si}$

interface (Fig. 6c) through

$$\chi = \frac{\arctan(\sin \Delta\chi)}{\cos(\Delta\chi) - d_p} \tag{1}$$

Indeed, on Si(001), a $(404)_{C54}$ plane only needs a tilt of 2.2° to align with $(113)_{Si}$, whereas a tilt of 3.2° is required to compensate the difference in Δd with $(222)_{Si}$, despite the relatively smaller Δd of the latter alignment. Therefore, the evaluation of an axiotaxial alignment should not only focus on the difference in d-spacing, but also include the dependence of $\Delta\chi$ on the inclination angle χ to obtain a lattice match at the interface.

Epitaxial alignment

The high intensity spots on the pole figures indicate *epitaxial* alignment of the thin film. An epitaxial alignment completely fixes the relative orientation of a crystalline grain with respect to the single crystal substrate, thus elim-

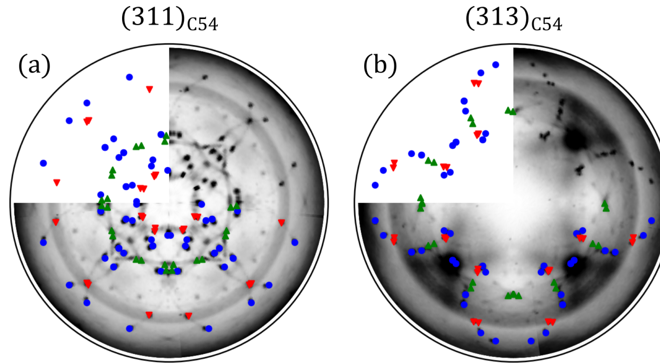

Figure 8: Pole figures overlayed with identified epitaxial features for data from a C54-$TiSi_2$ sample with an as-deposited Ti thickness of 8 nm.

inating the rotational symmetry. Therefore, a diffracting $\{hkl\}$ plane within
160 each epitaxial-oriented grain will also have a specific orientation which translates into local spots of high diffracted intensity on the pole figure. A total of three epitaxial orientations were identified (Fig. 7) and the relative orientation of each was determined with respect to the Si substrate (Tab. 3). Intriguingly, all observed spots of high intensity are in fact located along axiotaxial features,
165 a relationship which shall be discussed further on. For C54 films formed from a thinner 8 nm Ti layer, the axiotaxial features are barely visible, while the epitaxial features are very intense (Fig. 8). These epitaxies are identical to the epitaxies determined for films originating from the 30 nm Ti film (Tab. 3).

3.2. Texture on Si(111)

170 The preferential alignment between the C54-film and the Si(111) substrate is characterized by circular and epitaxial features (Fig. 9). Some of these circles, those associated with planar alignment of the planar alignment of $(404)_{C54}$ $\sim//(222)_{Si}$, are observed for both thickness. However, other preferential orientations are significantly different and therefore shall be discussed separately for
175 each thickness.

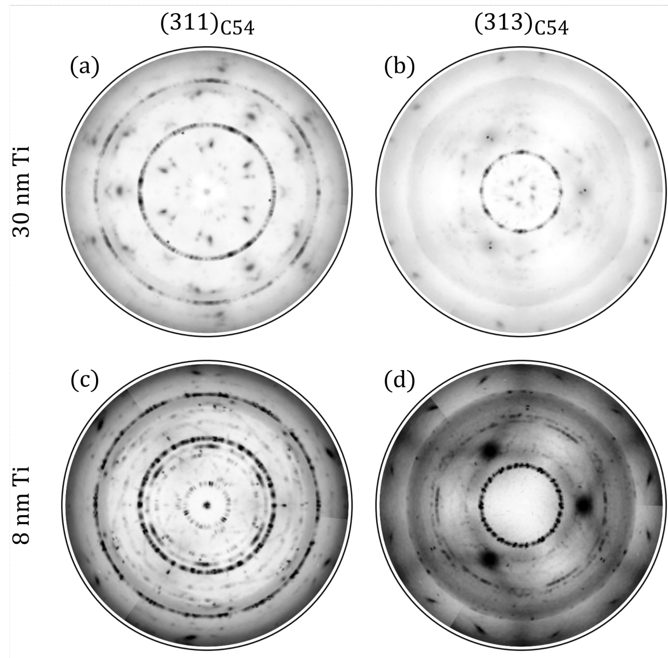

Figure 9: Pole-figure data of two C54-$TiSi_2$ diffraction planes as measured from a sample with an as-deposited Ti thickness of 30 nm (**a,b**) and 8 nm (**c,d**) on Si(111).

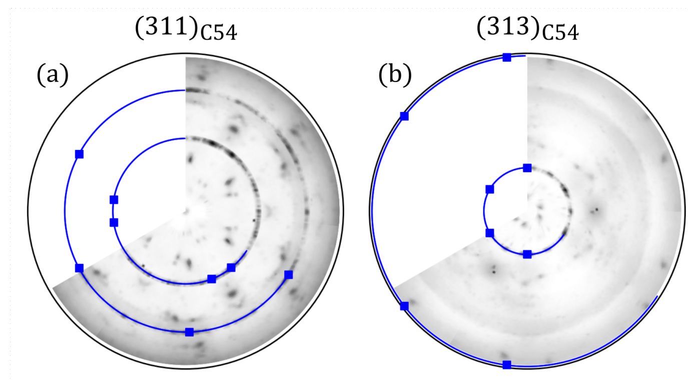

Figure 10: Pole figures from a C54-$TiSi_2$ sample with an as-deposited Ti thickness of 30 nm on Si (111). The measurement is overlayed with a $(404)_{C54}//(222)_{Si}$ fiber-like texture, together with an epitaxy partly coinciding with this axiotaxy.

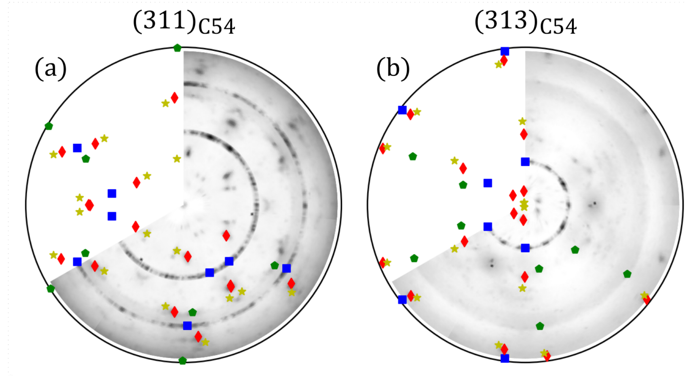

Figure 11: Additional epitaxial features are present for C54-$TiSi_2$ sample with an as-deposited Ti thickness of 30 nm on Si(111).

Texture for 30 nm *Ti*

The concentric circles for the thickest films can be explained by supposing a $(404)_{C54} \sim//(222)_{Si}$ axis of rotation (Fig. 10). Remarkably, the diffraction intensity varies as a function of ϕ along the ring, which is unusual for fiber-
180 textures. Moreover, the width of the concentric rings is very small (i.e. $<$ 2°FWHM), whereas the width of a fiber-texture usually is much broader (i.e. $>$ 5°FWHM, [13, 25], an observation related to the physical differences between a fiber texture and an axiotaxial texture).The driving force for a traditional fiber texture is usually a realization of surface energy. Here, it seems more plausible
185 to interpret the apparent fiber texture based on axiotaxy-type plane matching *across* the interface, as the $(404)_{C54}$ and $(222)_{Si}$ planes only differ by 0.06 Å. Evidently, such plane-to-plane matching would not be possible on a perfectly flat interface, as the planes would be parallel to the flat interface, and therefore never meet edge-to-edge. The small miscut of the Si(111) wafer would only
190 introduce one terrace-edge every 1 µm and cannot explain this effect. However, it was previously reported that C54-$TiSi_2$ can heavily agglomerate on Si(111) [15], resulting in a very rough interface.

A total of four epitaxial orientations are identified for this film (Fig. 11), and their orientation with respect to the Si substrate was determined (Tab. 4).

Table 4: Overview of observed epitaxial components of C54-$TiSi_2$/Si(111) for C54-films grown from 30 nm (A-D) and 8 nm (A, E) Ti.

Epitaxy (Symb.)	1st alignm.	2nd alignm.	Fig.
$A_{Si(111)}$ (■)	$(404)_{C54} \sim//(222)_{Si}$	$(050)_{C54} \sim//(220)_{Si}$	11
$B_{Si(111)}$ (●)	$(300)_{C54} \sim//(\bar{1}11)_{Si}$	$(\bar{2}0\bar{2})_{C54} \sim//(0\bar{1}\bar{1})_{Si}$	11
$C_{Si(111)}$ (♦)	$(01\bar{2})_{C54} \sim//(1\bar{1}\bar{1})_{Si}$	$(110)_{C54} \sim//(100)_{Si}$	11
$D_{Si(111)}$ (⋆)	$(\bar{2}10)_{C54} \sim//(1\bar{1}\bar{1})_{Si}$	$(110)_{C54} \sim//(00\bar{1})_{Si}$	11
$E_{Si(111)}$ (×)	$(500)_{C54} \sim //(222)_{Si}$	$(001)_{C54} \sim //(10\bar{1})_{Si}$	12

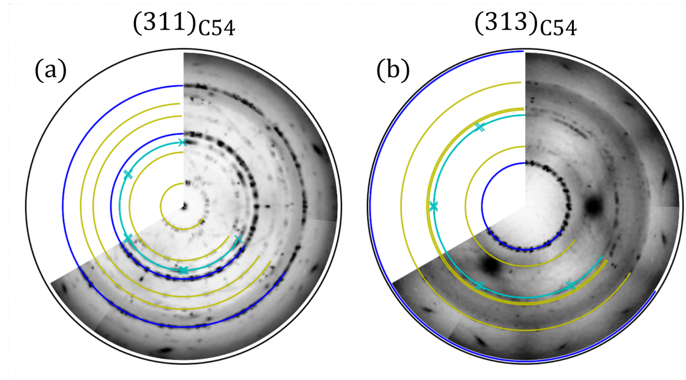

Figure 12: Additional epitaxial features are present between a C54-$TiSi_2$ film originating from a 8 nm Ti film on Si(111).

195 *Texture for* 8 nm *Ti*

Different axiotaxial and epitaxial textures are observed after annealing a thinner Ti layer on Si(111). In addition to the $(404)_{C54} \sim//(222)_{Si}$ fiber-like features (Fig 12, blue curve), we can also observe fiber-like rings originating from $(500)_{C54} \sim//(222)_{Si}$ (Fig 12, cyan curve) and $(511)_{C54} \sim//(222)_{Si}$ (Fig.
200 12, yellow curve), although the intensity of the latter alignment is significantly lower than the other fiber-like features. Again, the width of these concentric circles, as well as the variable intensity along ϕ suggests that these textures are in fact axiotaxial alignments with the substrate, where Table 5 gives an overview of the coinciding lattice planes.

Table 5: Fitted axiotaxial texture components between C54-$TiSi_2$ and Si(111) substrate.

	Symmetry Axis	χ_{obs} (°)	**d-spacing** (Å)	Δ d (%)	**Figure** (color)
	Si(222)	0	1.57	-	-
$\alpha_{Si(111)}$	C54(404)	0	1.51	4.2	10, 12 (blue)
$\beta_{Si(111)}$	C54(511)	0	1.56	0.0	12 (yellow)
$\eta_{Si(111)}$	C54(500)	0	1.65	5.1	12 (cyan)

205 All three fiber-like orientations are defined by a parallelism with similar planar spacings in film and substrate. The fiber-like circles also exhibit significant variation in diffraction intensity along ϕ, again indicating a preferential alignment closer towards an epitaxial orientation. Bright spots on the circles related to $(500)_{C54} \sim//(222)_{Si}$ can be explained by introducing $(004) \sim //(02\bar{2})$ as 210 a secondary orientation condition. This epitaxial orientation was previously reported (Tab. 1), and now the arc-shape revealed by the higher-resolution synchrotron pole figures indicates a dependence on the axiotaxial orientation. The bright spots along the $(404)_{C54} \sim //(222)_{Si}$ fiber-axis cannot be explained by a single additional constraint, but also correspond to the many epitaxial 215 orientations observed by Catana *et al.* [15], listed also in Table 1.

It is interesting to note that the $(511)_{C54}$ plane now aligns with $(222)_{Si}$, instead of $(113)_{Si}$ as reported earlier for the Si(001) substrate. We can again understand this when considering the alignment of the substrate planes with respect to the interface (Fig. 6c), where χ of $(222)_{Si}$ is lower on Si(111) than 220 on Si(001)-oriented substrates (0 and 54.7°, respectively), and thus the alignment requires a smaller tilt $\Delta\chi$ on Si(111) to compensate for the small lattice mismatch.

A question remains: which bonding is favoured as to explain the observed preferential orientations, i.e. which atoms are potentially bonding across the 225 interface. It is especially intreguing that some of the aligning planes have unsueally high indices, such as $(115)_{C54} \sim //(113)_{Si}$. The most reoccurring tex-

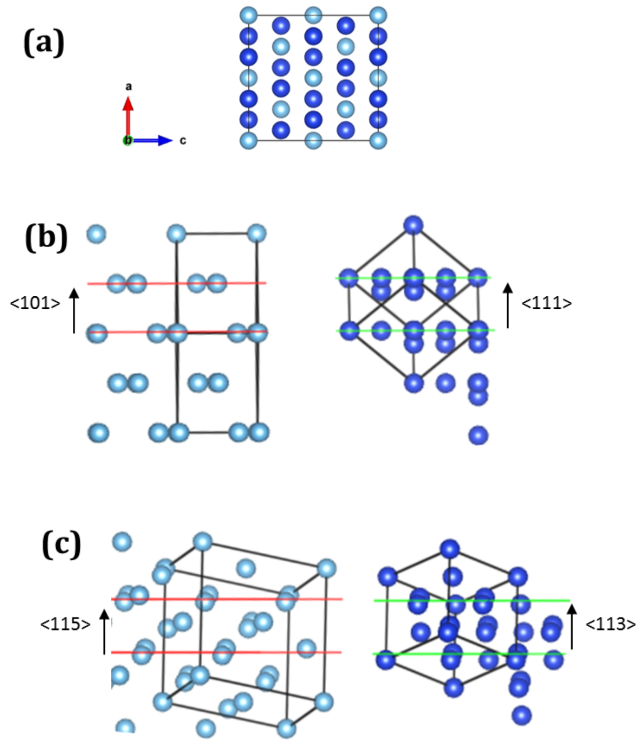

Figure 13: Image of the C54 unit cell (Ti: light blue, Si: dark blue). **(a)** The C54-$TiSi_2$ unit cell can aproximatly be described as a pseudo-tetragonal unit cell since $a \approx c$ (neglecting the positioning of the Si atoms). Hence explaining the observed symmetry between the a and c axis for several observed preferential orientations. **(b)** The interface determined by $(404)_{C54}//(222)_{Si}$ enables matching between nearly-closed packed Ti-atoms from the C54 silicide and the Si atoms of the substrate. **(c)** Other axiotaxial alignments, such as $(115)_{C54}//(222)_{Si}$, can also be described as a function of nearly-closed-packed Ti planes within the silicide.

ture, $(404)_{C54} \sim //(222)_{Si}$, has been discussed previously by Catana *et al.*, where the orientation was interpreted as favourable due to the presence of Ti-planes from C54-$TiSi_2$ along $\{101\}_{C54}$ with similar d-spacing and densities as
230 the {111} planes of Si [15]. By focusing on the Ti atoms, we can also explain the observed symmetry with respect to the a and c axis of the C54-unit cell (e.g. axiotaxies $\alpha_{Si(100)}$, $\alpha'_{Si(100)}$, $\beta_{Si(100)}$ & $\gamma_{Si(100)}$, $\alpha_{Si(111)}$ or epitaxies $A_{Si(001)}$, $A_{Si(001)}$, $A_{Si(111)}$, $C_{Si(001)}$ & $D_{Si(001)}$). Indeed, the C54-unit cell can be described as symmetrical in a and c, or even pseudo-tetragonal, when only
235 assessing the positions of the Ti-atoms, since $a = 8.26\,\text{Å} \approx c = 8.55\,\text{Å}$ (Fig. 13a). The simplification to mainly look at the Ti-atoms of the silicide phase, allows to understand the bonding across the interface indeed shows a continuation of nearly-closed-packed Ti-planes from the silicide to nearly-closed packed Si-planes from the substrate, as illustrated in Fig. 13b and c for orientations
240 containing both low-index and high-index silicide directions.

4. Conclusions

The preferential orientation between C54-$TiSi_2$ films and Si(001) and Si(111) substrates was investigated through high-angular-resolution synchrotron XRD pole figures. This enabled us to identify the axiotaxial texture in the C54-
245 $TiSi_2$/Si system, in addition to known epitaxial alignments. The majority of the observed epitaxies are in fact special cases of the same $(404)_{C54} \sim //(222)_{Si}$ axiotaxial alignment, indicating the importance of this plane-to-plane matching along the interface. From the diffraction intensities, one can derive that a lower Ti thickness corresponds with a higher fraction of the C54 grains with
250 an epitaxial orientation. The evaluation of the observed alignment indicates evaluate the stability of heterophase interfaces in terms of plane alignment and film thickness.

5. Acknowledgement

The authors acknowledge the FWO Vlaanderen, the Hercules foundation and BOF-UGent (GOA 01G01513) for providing financial support for this work. This research used resources of the National Synchrotron Light Source, a U.S. Department of Energy (DOE) Office of Science User Facility operated for the DOE Office of Science by Brookhaven National Laboratory under Contract No. DE-AC02-98CH10886.

References

References

[1] S. Zhang, M. Östling, Metal silicides in CMOS technology: past, present, and future trends, Critical Reviews in Solid State and Materials Sciences 28 (1) (2003) 1–129.

[2] L. Chen, Silicide technology for integrated circuits, Vol. 5, The Institution of Electrical Engineers, 2004.

[3] N. Breil, C. Lavoie, A. Ozcan, F. Baumann, N. Klymko, K. Nummy, B. Sun, J. Jordan-Sweet, J. Yu, F. Zhu, et al., Challenges of nickel silicidation in CMOS technologies, Microelectronic Engineering 137 (2015) 79–87.

[4] P. Adusumilli, A. Carr, A. Ozcan, C. Lavoie, J. Jordan-Sweet, D. Prater, N. Breil, S. Polvino, M. Raymond, D. Deniz, et al., Formation and microstructure of thin Ti silicide films for advanced technologies, in: 2016 IEEE International Interconnect Technology Conference/Advanced Metallization Conference (IITC/AMC), IEEE, 2016, pp. 139–140.

[5] Y. Yang, N. Breil, C. Yang, J. Hsieh, F. Chiang, B. Colombeau, B. Guo, K. Shim, N. Variam, G. Leung, et al., Ultra low p-type SiGe contact resistance FinFETs with Ti silicide liner using cryogenic contact implantation amorphization and Solid-Phase Epitaxial Regrowth (SPER), in: VLSI Technology, 2016 IEEE Symposium on, IEEE, 2016, pp. 1–2.

280 [6] H. Yu, M. Schaekers, A. Hikavyy, E. Rosseel, A. Peter, K. Hollar, F. Khaja, W. Aderhold, L. Date, A. Mayur, et al., Ultralow-resistivity CMOS contact scheme with pre-contact amorphization plus Ti (germano-) silicidation, in: VLSI Technology, 2016 IEEE Symposium on, IEEE, 2016, pp. 1–2.

[7] C. Chou, C. Chen, K. Chen, S. Teng, J. Huang, Y. Wu, Improved Current
285 Drivability for Sub-20-nm N-FinFETs by Ge Pre-Amorphization in Contact With Reverse Retrograde Profile, IEEE Electron Device Letters 38 (3) (2017) 299–302. doi:10.1109/LED.2017.2647957.

[8] K. Zhu, W. Ma, K. Wei, Y. Lei, J. Hu, T. Lv, Y. Dai, Separation mechanism of TiSi2 crystals from a Ti-Si eutectic alloy via directional solidification,
290 Journal of Alloys and Compounds 750 (2018) 102–110.

[9] D. Deduytsche, C. Detavernier, R. Van Meirhaeghe, C. Lavoie, High-temperature degradation of NiSi films: Agglomeration versus $NiSi_2$ nucleation, Journal of Applied Physics 98 (3) (2005) 033526.

[10] C. Detavernier, J. Jordan-Sweet, C. Lavoie, Texture of NiSi films on Si
295 (001),(111), and (110) substrates, Journal of Applied Physics 103 (11) (2008) 113526.

[11] A. Schrauwen, K. Van Stiphout, J. Demeulemeester, B. De Schutter, W. Devulder, C. Comrie, C. Detavernier, K. Temst, A. Vantomme, The role of composition and microstructure in Ni-W silicide formation and low
300 temperature epitaxial $NiSi_2$ growth by premixing Si, Journal of Physics D: Applied Physics 50 (6) (2017) 065303.

[12] R. Tung, J. Poate, J. Bean, J. Gibson, D. Jacobson, Epitaxial silicides, Thin Solid Films 93 (1) (1982) 77–90.

[13] B. De Schutter, K. De Keyser, C. Lavoie, C. Detavernier, Texture in thin
305 film silicides and germanides: A review, Applied Physics Reviews 3 (3) (2016) 031302.

[14] M. Fung, H. Cheng, L. Chen, Localized epitaxial growth of C54 and C49 $TiSi_2$ on (111) Si, Applied Physics Letters 47 (12) (1985) 1312–1314.

[15] A. Catana, P. Schmid, M. Heintze, F. Levy, P. Stadelmann, R. Bonnet, Atomic scale study of local $TiSi_2$/Si epitaxies, Journal of Applied Physics 67 (4) (1990) 1820–1825.

[16] I. Wu, J. Chu, L. Chen, Local epitaxy of $TiSi_2$ on (111) Si: Effects due to rapid thermal annealing and to the annealing atmosphere, Journal of Applied Physics 60 (9) (1986) 3172–3175.

[17] A. Özcan, K. Ludwig Jr, P. Rebbi, C. Lavoie, C. Cabral Jr, J. Harper, Texture of $TiSi_2$ thin films on Si (001), Journal of Applied Physics 92 (9) (2002) 5011–5018.

[18] I. Jauberteau, R. Mayet, J. Cornette, D. Mangin, A. Bessaudou, P. Carles, J. Jauberteau, A. Passelergue, Silicides and Nitrides Formation in Ti Films Coated on Si and Exposed to (Ar-N2-H2) Expanding Plasma, Coatings 7 (2) (2017) 23.

[19] V. Svilan, K. Rodbell, L. Clevenger, C. Cabral, R. Roy, C. Lavoie, J. Jordan-Sweet, J. Harper, Dependence of crystallographic texture of C54 $TiSi_2$ on thickness and linewidth in submicron CMOS structures, in: MRS Proceedings, Vol. 427, Cambridge Univ Press, 1996, p. 53.

[20] M. Bhaskaran, S. Sriram, K. Short, D. Mitchell, A. Holland, G. Reeves, Characterization of C54 titanium silicide thin films by spectroscopy, microscopy and diffraction, Journal of Physics D: Applied Physics 40 (17) (2007) 5213.

[21] M. Zhang, D. Qiu, P. Kelly, Crystallography of$TiSi_2$ (C54) epitaxy on (111) Si and (001) Si surfaces, Thin Solid Films 516 (16) (2008) 5498–5502.

[22] C. Detavernier, A. Özcan, J. Jordan-Sweet, E. Stach, J. Tersoff, F. Ross, C. Lavoie, An off-normal fibre-like texture in thin films on single-crystal substrates, Nature 426 (6967) (2003) 641–645.

335 [23] V. Kolosov, A. Thölen, Transmission electron microscopy studies of the specific structure of crystals formed by phase transition in iron oxide amorphous films, Acta Materialia 48 (8) (2000) 1829–1840.

[24] S. Gaudet, K. De Keyser, S. Lambert-Milot, J. Jordan-Sweet, C. Detavernier, C. Lavoie, P. Desjardins, Three dimensional reciprocal space mea- 340 surement by x-ray diffraction using linear and area detectors: Applications to texture and defects determination in oriented thin films and nanoprecipitates, Journal of Vacuum Science & Technology A 31 (2) (2013) 021505.

[25] S. Gaudet, P. Desjardins, C. Lavoie, The thermally-induced reaction of thin Ni films with Si: Effect of the substrate orientation, Journal of Applied 345 Physics 110 (11) (2011) 113524.

[26] K. De Keyser, C. Detavernier, Gustav: Ghent University Software for Texture Analysis and Visualisation, `http://www.cocoon.ugent.be/content/gustav/`.

[27] B. De Schutter, K. De Keyser, C. Detavernier, Visualization and classifi- 350 cation of epitaxial alignment at hetero-phase boundaries, Thin Solid Films 599 (2016) 104–112.